Astrophysical Journal, accepted
Preprint typeset using LaTeX style emulateapj v. 10/09/06

MERGING COLD FRONTS IN THE GALAXY PAIR NGC 7619 AND NGC 7626

S. W. Randall[1], C. Jones[1], R. Kraft[1], W. R. Forman[1], and E. O'Sullivan[1]

Astrophysical Journal, accepted

ABSTRACT

We present results from *Chandra* observations of the galaxy pair NGC 7619 and NGC 7626, the two dominant members of the Pegasus group. The X-ray images show a brightness edge associated with each galaxy, which we identify as merger cold fronts. The edges are sharp, and the axes of symmetry of the edges are roughly anti-parallel, suggesting that these galaxies are falling towards one another in the plane of the sky. The detection of merger cold fronts in each of the two dominant member galaxies implies a merging subgroup scenario, since the alternative is that the galaxies are falling into a pre-existing $\sim$ 1 keV halo without a dominant galaxy of its own, and such objects are not observed. We estimate the 3D velocities from the cold fronts and, using the observed radial velocities of the galaxies, show that the velocity vectors are indeed most likely close to the plane of the sky, with a relative velocity of $\sim$ 1190 km s^{-1}. The relative velocity is consistent with what is expected from the infall of two roughly equal mass subgroups whose total viral mass equals that of the Pegasus group. We conclude that the Pegasus cluster is most likely currently forming from a major merger of two subgroups, dominated by NGC 7619 and NGC 7626. NGC 7626 contains a strong radio source, a core with two symmetric jets and radio lobes. Although we find no associated structure in the X-ray surface brightness map, the temperature map reveals a clump of cool gas just outside the southern lobe, presumably entrained by the lobe, and possibly an extension of cooler gas into the lobe itself. The jet axis is parallel with the projected direction of motion of NGC 7626 (inferred from the symmetry axis of the merger cold front), and the southern leading jet is foreshortened as compared to the northern trailing one, possibly due to the additional ram pressure encountered by the forward jet.

Subject headings: galaxies: clusters: general — galaxies: clusters: individual (Pegasus, U842) — X-rays: galaxies — galaxies: individual (NGC7619) — galaxies: individual (NGC7626)

1. INTRODUCTION

Cluster mergers play a major role in determining the properties of the intracluster medium (ICM) of galaxy groups and clusters. They drive, and aid in the study of, several important physical processes in the ICM, including shock heating, the generation of relativistic particles, ram pressure stripping (and hence chemical enrichment of the ICM), magnetic fields, thermal conduction, and turbulence. *Chandra* has revealed the presence of cold fronts associated with several cluster mergers, where the cold central gas of the merging cluster forms a contact discontinuity with the ambient ICM. Cold fronts have been used extensively to study cluster mergers (for a review, see Markevitch & Vikhlinin 2007). In this paper, we examine the apparent merging cold fronts in the galaxy pair NGC 7619/NGC 7626.

NGC 7619 and NGC 7626 are the two dominant elliptical galaxy members of the Pegasus galaxy group (U842; Ramella et al. 2002). NGC 7619, which has a higher stellar velocity dispersion (336 km s^{-1} vs. 258 km s^{-1} Wegner et al. 2003), brighter absolute magnitude (22.94 vs. 22.87; Lauer et al. 2007), and is brighter in X-rays (4.3×10^{41} ergs s^{-1} vs. 1.2×10^{41} ergs s^{-1}; Fabbiano et al. 1992; Burstein et al. 1997; O'Sullivan et al. 2001), is presumably the more massive of the two galaxies. Woods et al. (2006) identify NGC 7619 as being paired with NGC 7617, which is a relatively weak X-ray source. Both NGC 7619 and NGC 7626 are radio sources, with NGC 7626 showing symmetric jets/lobes on either side of a central core (Birkinshaw & Davies 1985; Hibbard & Sansom 2003). NGC 7626 is notable for its unusual optical morphology and stellar velocity field in the core, which shows kinematically distinct shell-like regions (Jedrzejewski & Schechter 1988; Forbes & Thomson 1992; Balcells & Carter 1993). *Einstein* observations of this pair found X-ray emission from a diffuse halo associated with each galaxy (Fabbiano et al. 1992; Burstein et al. 1997), with a tail of asymmetric emission extending SW from NGC 7619. Subsequent *ROSAT* PSPC observations confirmed this asymmetry, which has been interpreted as arising from ram pressure stripping as NGC 7619 falls into the Pegasus group and interacts with the ICM (Trinchieri et al. 1997).

More recently, Kim et al. (2007; hereafter K07) presented results from *Chandra* and *XMM-Newton* observations of NGC 7619. They confirmed the presence of the stripped tail, and identified a sharp edge to the NE in the X-ray surface brightness profile. Based on this edge, they found a Mach number of $\sim$ 1 relative to the ICM. Abundances and temperatures determined from a spectral analysis of the tail indicate that this material has indeed been stripped from NGC 7619, and they interpret these results as directly observed evidence for the enrichment of the ICM as a result of ram pressure stripping.

We report here on *Chandra* observations of the NGC 7619/NGC 7626 pair. K07 have previously pre-

[1] Harvard-Smithsonian Center for Astrophysics, 60 Garden St., Cambridge, MA 02138, USA

sented results based on *XMM-Newton* and *Chandra* ACIS-S observations only of NGC 7619. We therefore focus on *Chandra* ACIS-I observations of this pair, and compare our results for NGC 7619 with those of K07 where appropriate. We give new results for NGC 7626, and for its interaction with NGC 7619. The observations and data reduction techniques are described in § 2. The X-ray image is presented in § 3, and results on temperature and abundance structure from spectral analysis are given in § 4. In § 5, we give new results for the structure and velocity of the cold front in NGC 7626, show that NGC 7619 and NGC 7626 are falling towards one another along an axis that is roughly in the plane of the sky, and argue that the Pegasus group is currently forming due to a major merger of two subgroups. Our results are summarized in § 6.

We assume a distance to the Pegasus cluster of 53 Mpc, based on results from surface brightness fluctuations for NGC 7619 (Tonry et al. 2001), which gives a scale of 0.25 kpc/″ for $\Omega_0 = 0.3$, $\Omega_\Lambda = 0.7$, and $H_0 = 70$ km s^{-1} Mpc^{-1}. All error ranges are 68% confidence intervals (i.e., 1-σ), unless otherwise stated.

2. OBSERVATIONS AND DATA REDUCTION

The NGC 7619/NGC 7626 pair was observed by *Chandra* on August 20, 2001, for 27 ksec with the *Chandra* CCD Imaging Spectrometer (ACIS), pointed such that each galaxy was visible on the front-side illuminated ACIS-I CCD array. NGC 7619 was again observed by *Chandra* for 40 ksec on September 24, 2003, this time pointed such that the galaxy was visible on the back-side illuminated S3 CCD. These data were reduced using the method described in Randall et al. (2008). All data were reprocessed from the level 1 events files using the latest calibration files (as of CIAO4.0). CTI and time-dependent gain corrections were applied where applicable. LC_CLEAN was used to remove background flares[2]. For the earlier ACIS-I observation, time bins that were not within 3σ of the mean were discarded. Unfortunately, the ACIS-S observation was badly contaminated by background flares. After periods with obvious flares were removed, the mean rate was calculated for observed quiescent time intervals, and LC_CLEAN was re-run, forcing the global mean to equal the quiescent rate. The resulting cleaned exposure times were 26.4 ksec and 16.6 ksec for the ACIS-I and ACIS-S observations, respectively.

The emission from NGC 7619, NGC 7626, and the surrounding Pegasus group fills the image field of view for each observation. We therefore used the standard CALDB[3] blank sky background files appropriate for each observation, normalized to our observations in the 10-12 keV energy band. To generate exposure maps, we assumed a MEKAL model with $kT = 1$ keV, Galactic absorption, and abundance of 30% solar at a redshift $z = 0.0125$, which is consistent with typical results from detailed spectral fits (see § 4).

3. THE X-RAY IMAGE

The exposure corrected, background subtracted, smoothed mosaic image is shown in Figure 1 (the optical *DSS* image of the same field is shown for comparison). Regions containing point sources were "filled in" using a Poisson distribution whose mean was equal to that of a local annular background region. The same image, but with point sources included, is shown in Figure 2 with *ROSAT* PSPC surface brightness contours overlain to show the extent of the diffuse emission in the Pegasus group, which fills the *Chandra* field of view. In the west, NGC 7619 shows a sharp edge to the northeast, and a diffuse, broad, ram pressure stripped tail, noted previously (Fabbiano et al. 1992; Trinchieri et al. 1997; K07). In the east, NGC 7626 also shows an edge in its diffuse emission to the southwest, but in this case there is no obvious stripped tail. The symmetry axes of the edges are roughly anti-parallel, i.e., the cold fronts are directed towards one another. The sharpness and relative orientation of the edges, along with the orientation of NGC 7619's stripped tail, immediately give the impression of two galaxies falling towards each other in the plane of the sky. The edges appear qualitatively similar to merger cold fronts seen in other systems (e.g., Markevitch et al. 2000; Vikhlinin et al. 2001; Machacek et al. 2005). We therefore investigate the possibility that this system shows the early stage of a major merger between two main subgroups, as opposed to one or more smaller subgroups falling into a preexisting cluster.

4. SPECTRAL ANALYSIS

The X-ray image suggests diffuse emission associated with NGC 7619, NGC 7626, and possibly diffuse emission from the Pegasus group filling the field of view. We generate a temperature map as a guide for detailed spectral fitting to disentangle the various components. We assume a galactic absorption of $N_H = 4.82 \times 10^{20}$ cm^{-2} throughout.

4.1. *Temperature Map*

The temperature map was derived using the same method as developed in Randall et al. (2008), similar to that employed by O'Sullivan et al. (2005) and Maughan et al. (2006). For each temperature map pixel, we extracted a spectrum from a circular region containing 1000 net counts (after subtracting the blank sky background). The resulting spectrum was fit in the 0.6 – 5.0 keV range with an absorbed APEC model using XSPEC, with the abundance allowed to vary. Maps were generated using the ACIS-I data only. The resulting temperature map is shown in Figure 3. Unfortunately, due to the small number of net counts, the extraction regions for the temperature map pixels were relatively large. Faint regions had extraction radii on the order of 4.1′ (61.5 kpc), while the brightest regions, near the galaxy cores, had radii of 14″ (3.5 kpc). As a result, each pixel in the temperature maps is highly correlated with nearby pixels, and the temperature map is effectively smoothed on large scales.

Nevertheless, clear structure is visible in the map. NGC 7619 and NGC 7626 are each associated with a cloud of cool gas, with central temperatures of $kT \approx 0.75$ keV. A cool region extends southwest from NGC 7619, in the direction of the stripped tail, and rises to a temperature of about $kT \approx 1$ keV, which is consistent with findings of K07 using *XMM-Newton* data. Higher temperature regions, presumably from diffuse group emission and with $kT \approx 1.2 - 1.3$ keV, can be

[2] http://asc.harvard.edu/contrib/maxim/acisbg/
[3] http://cxc.harvard.edu/caldb/

seen between the galaxies and surrounding NGC 7626. Although the observed surface brightness edges roughly correspond to regions of transition from cooler to hotter gas, the temperature maps are too smoothed to match these features in detail. An inspection of the error maps suggests that the hot spot ($kT \approx 1.6$ keV) to the north is statistically significant. While there are bright point sources in this region, most notably two unidentified sources that were detected as a single blended source in *ROSAT* PSPC observations (Trinchieri et al. 1997), these sources have been adequately masked out when generating the temperature map. If we remake the map with even larger point source masks the hot spot remains. We conclude that, although the fits in this area are statistically good fits, the hot spot may be an artifact of the method used to generate the temperature map due to the low number of net counts and resulting large extraction regions in this area. More detailed fits are discussed in § 4.2.

4.2. *Detailed Spectra*

Based on the derived temperature map and the X-ray image, we defined 10 regions for detailed spectral analysis. A summary of the regions and spectral model for each region are given in Table 1. R1 and R2 cover the central projected 12 kpc of NGC 7619 and NGC 7626, respectively. R3 and R4 are just inside and outside of the surface brightness edge to the northeast in NGC 7619, while R5 and R6 give the same values for the southwestern edge in NGC 7626. R7 is a featureless region to the north, and should include only group emission. Finally, R8, R9, and R10 cover the southern radio lobe (discussed in § 5.3), a region directly east of the lobe, and another west of the lobe, respectively. The regions are shown overlain on the X-ray image in Figure 4. The spectrum from each region was initially fit with an absorbed APEC model over the 0.6-5.0 keV range with the abundance allowed to vary. The fits to R1 and R2 showed an excess at hard energies, therefore a power-law component was included in the fits to these regions to account for the contribution from unresolved X-ray binaries. The best-fit photon indicies are are consistent with $\Gamma \approx 1.5$, as expected for a population of X-ray binaries (Sarazin et al. 2003). We found that including a second thermal component, in lieu of the power-law, gave an equally good fit to the data, though with a second temperature that was higher than would be expected from the diffuse group emission at ~ 1.2 keV. The results from the multiple thermal component fit for the core of NGC 7619 are given in Table 1 for comparison. We note that this hard energy excess is only detected in the galaxy cores and its precise nature is not relevant to our main results.

Table 1 shows a clear increase in temperature across each brightness edge, $0.83^{+0.02}_{-0.01}$ to $1.05^{+0.09}_{-0.05}$for NGC 7619, and $0.94^{+0.06}_{-0.08}$ to $1.50^{+0.48}_{-0.27}$ for NGC 7626, with the cooler gas in the brighter, interior regions. This clearly establishes these edges as cold fronts. The core of NGC 7619 is slightly hotter than that of NGC 7626, which is consistent with NGC 7619 being the more massive of the two galaxies. Using the fits to the detailed spectra, we can derive the approximate mass in cool gas in the core of each galaxy. Assuming a spherical geometry with a radius of 12 kpc, we find $M_{gas,\mathrm{N7619}} \approx 1 \times 10^{10}\,\mathrm{M}_\odot$ and $M_{gas,\mathrm{N7626}} \approx 5 \times 10^{9}\,\mathrm{M}_\odot$.

5. DISCUSSION

5.1. *Structure of the Cold Fronts*

The *Chandra* image (Figure 1) shows two sharp brightness edges, one northeast of NGC 7619, the other southwest of NGC 7626. Spectral analysis revealed temperature differences on either side of the edges, indicating that these edges are cold fronts (§ 4.2, Table 1). As such, we expect there to be a density discontinuity located at each edge. To measure the amplitude of these density jumps, we extracted the *Chandra* 0.6–5.0 keV surface brightness profile in two sectors, one for NGC 7619 and one for NGC 7626. The regions were defined such that the radii of curvature matched those of the edges. In neither case did the position of the center of curvature match that of the optical or X-ray emission central peak. The extraction regions are shown in Figure 5. We use only the ACIS-I data, since the profile for the edge associated with NGC 7619 has already been accurately measured and fit by K07 using *Chandra* ACIS-S and *XMM-Newton* data, and we mainly want to cross-check their results with our own from ACIS-I. In the case of NGC 7626, only ACIS-I data are available from *Chandra*.

The resulting emission measure profiles are shown in Figure 6 (distance is measured from the center of curvature of the apparent edge).These profiles were fit with a spherical gas density model consisting of two power laws. The free parameters were the normalization, the inner (α) and outer (β) slopes, the position of the density discontinuity (r_{break}), and the amplitude of the jump (A). The temperature and abundance for each bin was determined by fitting the projected emission in coarser bins over the same region, as there were insufficient counts to perform deprojected spectral fits. For the edge in NGC 7619, we find $\alpha = -0.45^{+0.23}_{-0.33}$, $\beta = -1.09^{+0.23}_{-0.24}$, $r_{\mathrm{break}} = 29^{+0.9}_{-1.2}$ kpc, and $A = 2.8^{+1.4}_{-0.2}$. This is consistent with results from K07, who find a jump in density of 4.1 ± 0.6 (90% confidence interval). For the edge in NGC 7626, we find similar results: $\alpha = -0.67^{+0.50}_{-0.21}$, $r_{\mathrm{break}} = 25^{+1.0}_{-1.0}$ kpc, and $A = 5.4^{+1.0}_{-0.4}$, where β was fixed at its best-fit value of $\beta = 0.55$. In each case, the two power law model was a much better fit to the data than a single power law or beta model. The best fit models are plotted in Figure 6.

One concern when considering the emission measure profiles is the contribution from the central galaxy gas, especially in the case of NGC 7626. A steep density gradient in the galactic gas will bias the inner bins high and possibly lead to an artificial increase in the amplitude of the density jump, particularly if the width of the bins is large compared to the scale of the system, as is the case here due to the relatively low photon statistics. As a test of the significance of this effect, we fit the emission measure profile of an identical region to the northwest of NGC 7626, at the same distance from the galactic center. In this case, the profile was well described by a single power-law, with a chi-squared per degree-of-freedom of $\chi^2_\nu = 0.6$ (for comparison, in the southwest a single power-law model gave $\chi^2_\nu = 4.8$, while the two power-law model gave $\chi^2_\nu = 0.3$). The two power-law model did not improve the chi-squared of the fit, and the amplitude and position of the density jump could not be

well-determined. This suggests that the central galactic gas does not strongly bias our measurement of the amplitude of the jump associated with the edge seen in the southwest.

There are several reasons to identify the edges as merger cold fronts, as opposed to sloshing fronts as described by Ascasibar & Markevitch (2006). The centers of curvature are not centered on the optical or X-ray brightness peaks, as should roughly be the case for sloshing fronts. The density jumps are large, in the range of a factor of 2–6, more characteristic of merger cold fronts than sloshing cold fronts, which typically have density jumps in the 1–1.5 range (Markevitch & Vikhlinin 2007). The inferred velocity of the subclumps is mildly supersonic relative to the ambient ICM (see § 5.2). While this is not impossible for sloshing fronts, it is more typical of merger fronts. Although we were unable to constrain abundance variations across the edges due to inadequate statistics, K07 found an abundance jump associated with the edge in NGC 7619 (which has very similar properties to the edge we observe in NGC 7626), indicating a merger cold front. Finally, although the errors are too large to be definitive, we find that the temperature *may* be slightly higher for the emission just outside the edge in NGC 7626 as compared to a blank region of sky to the north in the ACIS-I data (cf. R6 and R7 in Table 1), and to the ambient group temperature found by K07 of $kT \approx 1.1$ keV. This could indicate a weak shock in this region, though the errors are large, and if real the difference could be due to normal radial temperature variations in the ICM (further observations would be required to detect the presence of a shock front). We conclude that these features mostly likely represent merger cold fronts (as opposed to sloshing fronts), as previously concluded by K07 for NGC 7619.

5.2. *Geometry of the Merger*

Given the apparent sharpness of the cold front edges, and assuming that these are indeed merger cold fronts, we expect that the merger axes of NGC 7619 and NGC 7626 are close to the plane of the sky. As pointed out by Vikhlinin et al. (2001), the 3D velocity of a merger cold front can be determined by comparing the pressure in the subclump to the external pressure:

$$\frac{p_0}{p_1} = \left(1 + \frac{\gamma-1}{2} M_1^2\right)^{\frac{\gamma}{\gamma-1}}, \quad M_1 \leq 1, \tag{1}$$

$$\frac{p_0}{p_1} = \left(\frac{\gamma+1}{2}\right)^{\frac{\gamma+1}{\gamma-1}} M_1^2 \left(\gamma - \frac{\gamma-1}{2M_1^2}\right)^{\frac{-\gamma}{\gamma-1}}, \quad M_1 > 1, \tag{2}$$

where p_0 is the thermal pressure at the stagnation point (which is equal to the pressure within the subclump), p_1 is the thermal pressure in the external medium, M_1 is the Mach number of the subclump relative to the sound speed in the external medium, and $\gamma = 5/3$ is the adiabatic index of the gas (Landau & Lifshitz, 1959). Using the two power law density model found in § 5.1, we find a pressure jump across the cold front in NGC 7626 of $p_0/p_1 = 3.4^{+0.9}_{-1.2}$, which corresponds to a Mach number of $M = 1.4^{+0.2}_{-0.3}$ (where the 1-σ confidence intervals have been estimated by separately propagating the upper and lower confidence intervals on the density jump and temperatures). This result is close to $M \approx 1.2$, found by K07 for the apparently similar cold front in NGC 7619 (though they point out that if they take into account the change in abundance across the front they find $M \approx 0.9$). For comparison, using the ACIS-I data only (and accounting for abundance variations), we find $M = 1.06^{+0.32}_{-0.10}$ for NGC 7619.

Using the 3D velocity of the cold fronts in combination with the observed radial velocity of the galaxies one can estimate the orientation of the merger axes. For a sound speed of $c_s = 540$ km s^{-1} in the ambient gas (at $kT = 1.1$ keV), the 3D velocity of NGC 7626 relative to the ambient ICM is 648 km s^{-1}. The radial velocity is 3405 km s^{-1}, -121 km s^{-1} relative to the mean radial group velocity of 3525 km s^{-1} (Ramella et al. 2002). Assuming that the radial velocity relative to the group mean approximates the radial velocity relative to the ICM, we find that the direction of motion of NGC 7626 is about 10° from the plane of the sky. K07 find that the relative velocity vector of NGC 7619 is $25-30°$ from the plane of the sky, pointing into rather than out of the plane (its radial velocity of 3820 km s^{-1} is larger than the mean group radial velocity). If we assume that the projected directions of motion are along the symmetry axes of the cold fronts, we conclude that NGC 7626 and NGC 7619 are bound to the Pegasus group (assuming the virial mass of the group to be 8.0×10^{13}M$_\odot$ as given by Ramella et al. (2002)) and falling towards each other with a net relative velocity of approximately -1190 km s^{-1} (the projected impact parameter is relatively small, ~ 63 kpc).

The fact that NGC 7626 and NGC 7619, the two dominant members of the Pegasus group, are falling towards one another with velocities significantly different (as compared to the group velocity dispersion of 414 km s^{-1} given by Ramella et al. 2002) from the mean group velocity suggests that we are seeing a major merger between two similar-sized groups. If this is indeed the case, one might expect to see a double-peaked radial velocity distribution (although the offset of the peaks may not be large since the merger axis is close to the plane of the sky). Ramella et al. (2002) identify 13 members of the Pegasus group. Unfortunately, statistical analysis shows that there are an insufficient number of galaxies to distinguish between a single-peaked distribution and the bimodal distribution one would expect for two merging subgroups.

As a further test of this scenario, we estimated the infall velocity of the merging subgroups. We assumed that the total virial mass in the subgroups equals the total virial mass of the Pegasus group, which is given by Ramella et al. (2002) as 8.0×10^{13}M$_\odot$. The mass ratio of the subgroups was estimated from the ratio of the square of the galactic velocity dispersions given by Wegner et al. (2003). This assumes that the group mass scales with the dominant galaxy mass, which is not true in general, but suffices for our rough estimate here. This yielded viral masses of $M_{\rm N7619} = 5 \times 10^{13}M_\odot$ and $M_{\rm N7626} = 3 \times 10^{13}M_\odot$. Each subgroup was given an NFW potential (Navarro et al. 1995) with a concentration parameter derived from the relations given by Neto et al. (2007), normalized to give the assumed virial mass. The derived relative free-fall velocity at the ob-

served separation of 100 kpc was -960 km s^{-1}, which is on the order of the -1190 km s^{-1} we derive from cold front measurements. Relative to the center of mass, the velocity of the smaller subgroup was about 120 km s^{-1} higher than that of the larger group (540 km s^{-1} vs. 420 km s^{-1}), similar to what we derive for NGC 7626 and NGC 7619 (648 km s^{-1} vs. 540 km s^{-1}). While this test is inconclusive, the fact that the best-fit point values are in good agreement with our rough estimate indicates that our model is at least plausible.

This scenario assumes that the gas in the outer regions of the merging groups has already sufficiently mixed to form an ambient ICM that is at rest in the center of mass frame, since the cold fronts imply velocities relative to the ICM that are less than the relative velocity of the galaxies. In the case of an isolated galaxy filled with diffuse 0.75 keV gas that is falling into a group containing a central massive galaxy, one would expect the velocity implied by the cold front in the galaxy to equal the relative velocity of the two galaxies. In comparison, we find cold front velocities that are about half the estimated relative velocity of the galaxies. A cartoon showing how this can occur for two merging subgroups is shown in Figure 7. In panel *a*, the groups are falling towards one another, but the virial radii have yet to overlap. In panel *b* , the outer regions of the groups' extended halos merge subsonically, forming a region in between the groups that is at rest with respect the the center of mass of the system and is most likely heated due to adiabatic compression. As the groups continue to merge, the relative velocity becomes transonic, and, as shown in panel *c*, the central galaxies and their associated cool gas come into contact with the mixed ICM in between the groups to form ram pressure stripped tails and merger cold fronts. This scenario predicts a low abundance in the mixed group emission between NGC 7626 and NGC 7619 (as compared to the abundance in the ISM and the stripped tail), which is hinted at in our detailed spectral fits (see Table 1 and Figure 4).

We have suggested that the symmetry axes of the cold fronts indicates that this is not a head-on merger, with a projected impact parameter of ~ 63 kpc (see Figure 4). In this case, one expects a curved trajectory for each of the infalling subgroups. As shown in the left panel of Figure 1, and by the *ROSAT* contours in Figure 2, the stripped tail in NGC 7619 is displaced to the east, in the direction of NGC 7626, relative to the symmetry axis of the cold front, consistent with our merger scenario. We do not detect a stripped tail in NGC 7626, and therefore cannot confirm a curved trajectory. The lack of an obvious stripped tail in this system may be due to its smaller mass and higher velocity relative to ICM (inferred above) as compared to NGC 7619, resulting in the gas in the extended halo being stripped away at an earlier stage of the merger.

Finally, we note that the presence of merger cold fronts in the two most dominant galaxies in the Pegasus group alone suggests our merging subgroups scenario. If we were witnessing, for instance, NGC 7619 falling into a group dominated by NGC 7626, we would expect to see the ram pressure stripped tail and merger cold front in NGC 7619, however we would not expect to find a merger cold front in NGC 7626 (though we may find a sloshing cold front). We note that the existence of the density jump in NGC 7626 is well determined, with an amplitude of the jump being *at least* a factor of 5 ($1-\sigma$ confidence). This, along with the temperature difference across the edge, which is also well determined, suggests that the brightness edge in NGC 7626 represents a merger cold front. The only alternative scenario consistent with finding two merger cold fronts would be that both NGC 7626 and NGC 7619 are falling into a pre-existing cloud of 1 keV gas that had no associated dominant galaxy of its own. The authors are unaware of such an object being detected in the *RASS* or other surveys. We conclude that the data are fully consistent with the scenario of a major merger between two subgroups with a small impact parameter.

5.3. *Radio Lobes in NGC 7626*

NGC 7626 is a well-known radio source, with symmetric jets on either side of a central core (Birkinshaw & Davies 1985; Hibbard & Sansom 2003). Figure 8 shows VLA 20 cm radio observations of these jets and their associated lobes along side the *Chandra* X-ray image with the NRAO VLA Sky Survey (NVSS, Condon et al. 1998) contours overlain. The compact central radio source in NGC 7619 can be seen to the west. There is no obvious structure in the X-ray surface brightness associated with the southern lobe (the northern lobe is outside the field of view). Figure 9 shows the temperature map discussed in § 4.1 with the same NVSS radio contours overlain. A clump of cool gas can be seen just to the south of the lobe, the northern boundary of which roughly follows the radio contours. Furthermore, there is an extension of cool gas into the core of the lobe, suggesting the presence of cool gas within the lobe itself. For a more detailed comparison, we fit the spectrum of a circular region encompassing the southern lobe (R8 in Table 1) and to two other identical regions just to the east (R9) and west (R10). R10 contains the cool clump south of the lobe, and some of the ram pressure stripped tail of NGC 7619. The results of these fits are given in Table 1. Unfortunately, there are too few counts in these regions to constrain temperature differences, and we are left with the variations suggested by the overlapping regions used to generate the temperature map.

As shown in Figure 8, the jets are roughly aligned with the axis of symmetry of the cold front, i.e., the presumed projected direction of motion. As is most clearly seen from the contours in the left panel of Figure 8, the jets are not completely symmetric, with the southern jet being about $1.7'$(25 kpc) shorter than the northern jet ($5.78'$ (87 kpc) vs. $7.46'$ (112 kpc)). Although this does not necessarily imply our merger scenario, we note that it is at least consistent, in that the foreshortening of the southern jet may be due to the additional ram pressure force this jet sees as it pushes into the ICM in the direction of motion. If we extrapolate our density model for NGC 7626 given in § 5.1 (and shown in Figure 6) to the tip of the southern lobe, we find the ram pressure at this point to be $\sim 3 \times 10^{-12}$ dyne cm^{-2} for an object moving with NGC 7626 at 648 km s^{-1} (derived in § 5.2). For an outward moving lobe, the ram pressure on the lobe would be larger due to the additional velocity of the lobe relative to the ICM. Alternatively, the jet seems to extend to the edge of the ram pressure stripped tail of NGC 7619, and may be turned back by the cooler, more

dense gas there. The cool clump of the gas south of the lobe could either be material that has been pushed out of NGC 7626 by the radio lobe, or entrained gas from the ram pressure stripped tail of NGC 7619. A deeper X-ray observation of this region (and the region near the northern lobe) to examine the interaction of the radio jets and the ambient ICM would be of interest.

6. SUMMARY

We interpreted *Chandra* observations of the Pegasus group in the context of a major merger of two subgroups, dominated by NGC 7619 and NGC 7626. Sharp surface brightness edges in each galaxy are suggestive of merger (as opposed to sloshing) cold fronts, due the the temperature changes across the edges, the high amplitude of the associated density jumps, the large inferred velocities, and the offsets between the centers of curvature of the features and the X-ray brightness peaks. K07 previously reached a similar conclusion for the edge in NGC 7619. The axes of symmetry of the fronts are roughly antiparallel, and each velocity vector is found to be close to the plane of the sky, implying that these systems are infalling towards one another. The relative velocity of the galaxies is consistent with what is expected for two roughly equal mass subgroups in free fall with a zero impact parameter. Although the 3D velocities derived from the cold fronts are uncertain, the detection of the cold fronts (i.e., the temperature and density jumps across the edges) is not. If these are indeed merger cold fronts, the presence of these fronts alone would suggest a merging subgroup scenario, since the alternative would be two galaxies falling into a pre-existing 1 keV cloud that did not contain a dominant galaxy. Such objects are not observed. The temperature map shows a clump of cool gas that is apparently entrained by the southern lobe, and some cooler gas within the lobe itself. The cool clump may have been pushed out of NGC 7626 by the jet, or formed by pile up when the lobe encountered the ram pressure stripped tail of NGC 7619. Finally, the southern radio jet in NGC 7626 is foreshortened, which may be due to the additional ram pressure from the merger, or to encountering the denser material in the ram pressure stripped tail of NGC 7619, as it interacts with the ambient ICM.

All the data discussed above are fully consistent with our interpretation of a major merger currently forming the Pegasus group. Other interpretations may also be consistent with the data, e.g., NGC 7626 merging into an existing group whose dominant central galaxy NGC 7619 is undergoing large "sloshing motions" as a result of the merger. For the reasons detailed above, e.g., the large amplitude of the density jumps associated with the cold fronts, we argue that the double merger is more likely. Further observations, that would provide more accurate spectral data allowing more detailed and precise hydrodynamic models, may be able to definitively discriminate among the alternatives. In addition, since major group mergers may show more extreme features in the gas relative to cluster mergers (e.g. larger pressure jumps, larger relative displacements between the central galaxy and any gas, etc.), more simulations of group mergers would be useful.

The financial support for this work was partially provided for by the NASA *Chandra* grant GO0-1026X, the Chandra X-ray Center through NAS8-03060, and the Smithsonian Institution. We thank Pasquale Mazzotta for useful comments.

REFERENCES

Ascasibar, Y., & Markevitch, M. 2006, ApJ, 650, 102
Balcells, M., & Carter, D. 1993, A&A, 279, 376
Birkinshaw, M., & Davies, R. L. 1985, ApJ, 291, 32
Burstein, D., Jones, C., Forman, W., Marston, A. P., & Marzke, R. O. 1997, ApJS, 111, 163
Condon, J. J., Cotton, W. D., Greisen, E. W., Yin, Q. F., Perley, R. A., Taylor, G. B., & Broderick, J. J. 1998, AJ, 115, 1693
Fabbiano, G., Kim, D.-W., & Trinchieri, G. 1992, ApJS, 80, 531
Forbes, D. A., & Thomson, R. C. 1992, MNRAS, 254, 723
Hibbard, J. E., & Sansom, A. E. 2003, AJ, 125, 667
Jedrzejewski, R., & Schechter, P. L. 1988, ApJ, 330, L87
Kim, D.-W., Kim, E., Fabbiano, G., & Trinchieri, G. 2007, preprint (astro-ph/0706.4254v2; K07)
Landau, L. D., & Lifshitz, E. M. 1959, Fluid Mechanics, Permagon, London
Lauer et al. 2007, ApJ, 664, 226
Machacek, M., Dosaj, A., Forman, W. R., Jones, C., Markevitch, M., Vikhlinin, A., Warmflash, A., Kraft, R. 2005, ApJ, 601, 221
Markevitch, M. et al. 2000, ApJ, 541, 542
Markevitch, M., & Vikhlinin, A. 2007, PhR, 443, 1
Maughan, B. J., Ellis, S. C., Jones, L. R., Mason, K. O., Crdova, F. A., & Priedhorsky, W. 2006, ApJ, 640, 219
Navarro, J. S., Frenk, C. S., & White, S. D. M. 1995, MNRAS, 275, 720
Neto et al. 2007, MNRAS, 381, 1450
O'Sullivan, E., Vrtilek, J. M., Kempner, J. C., David, L. P., & Houck, J. C. 2005, MNRAS, 357, 1134
O'Sullivan, E., Forbes, D. A., & Ponman, T. J. 2001, MNRAS, 328, 461
Ramella, M., Geller, M. J., Pisani, A., & da Costa, L. N. 2002, AJ, 123, 2976
Randall, S., Nulsen, P., Forman, W., Jones, C., Machacek, M., Murray, S., & Maughan, B. 2008, ApJ, 688, accepted
Sarazin, C. L., Kundu, A., Irwin, J. A., Sivakoff, G. R., Blanton, E. L., & Randall, S. W. 2003, ApJ, 595, 743
Tonry, J. L., Dressler, A., Blakeslee, J. P., Ajhar, E. A., Fletcher, A. B., Gerard, A. L., Metzger, M. R., & Moore, C. B. 2001, ApJ, 546, 681
Trinchieri, G., Fabbiano, G., & Kim, D.-W. 1997, A&A, 318, 361
Vikhlinin, A., Markevitch, M., & Murray, S. 2001, ApJ, 551, 160
Wegner, G., et al. 2003, AJ, 126, 2268
Woods, D. F., Geller, M. J., & Barton, E. J. 2006, AJ, 132, 197

TABLE 1
Spectral Fits

Region #	CCDs	kT (keV)	Abund. (solar)	Γ	χ^2/dof	Net Cnts.
R1	ACIS-I/S3	$0.778^{+0.008}_{-0.008}$	$0.77^{+0.90}_{-0.22}$	$1.81^{+0.38}_{-0.52}$	112/90=1.33	4938
R1	ACIS-I/S3	$0.774^{+0.008}_{-0.010}/3.34^{+2.41}_{-0.88}$	$0.76^{+0.54}_{-0.12}$		109/83=1.32	4938
R2	ACIS-I	$0.630^{+0.031}_{-0.028}$	$0.16^{+3.96}_{-0.07}$	$1.09^{+0.99}_{-1.08}$	15/19=0.79	1282
R3	ACIS-I/S3	$0.831^{+0.014}_{-0.015}$	$0.32^{+0.09}_{-0.07}$		44/36=1.22	1633
R4	ACIS-I/S3	$1.050^{+0.092}_{-0.047}$	$0.09^{+0.03}_{-0.02}$		79/54=1.58	1235
R5	ACIS-I	$0.938^{+0.066}_{-0.074}$	$0.10^{+0.05}_{-0.04}$		4/9=0.42	395
R6	ACIS-I	$1.500^{+0.486}_{-0.269}$	$0.16^{+0.52}_{-0.13}$		16/22=0.73	352
R7	ACIS-I	$1.263^{+0.351}_{-0.225}$	$0.11^{+0.16}_{-0.08}$		9/9=1.00	365
R8	ACIS-I	$1.358^{+0.178}_{-0.085}$	$0.55^{+0.75}_{-0.24}$		15/12=1.24	260
R9	ACIS-I	$1.116^{+0.531}_{-0.457}$	$0.04^{+0.24}_{-0.04}$		6/8=0.75	148
R10	ACIS-I	$1.068^{+0.125}_{-0.062}$	$0.24^{+0.22}_{-0.08}$		3/7=0.45	493

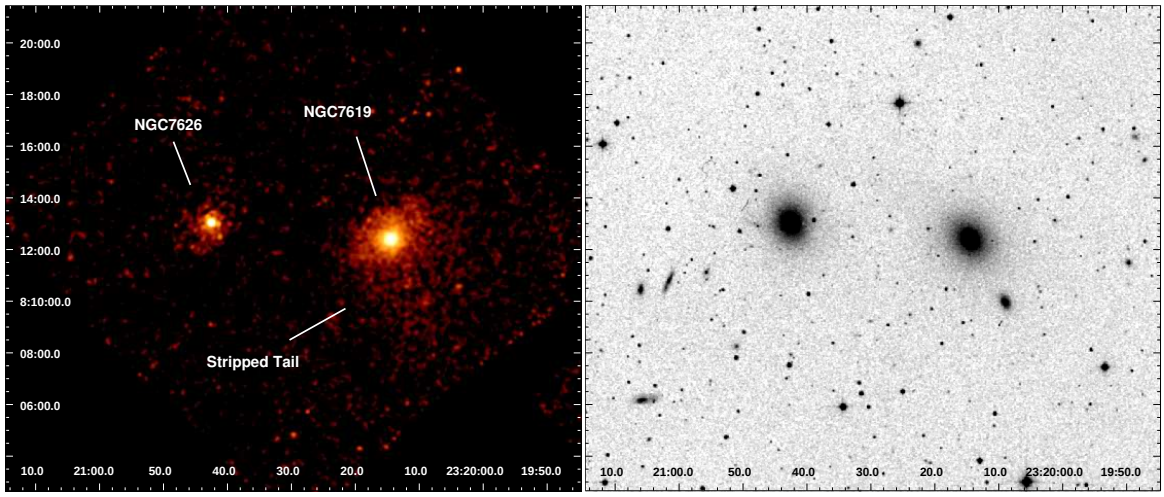

Fig. 1.— *Left Panel:* Exposure corrected, background subtracted 0.6–5 keV mosaic image of the *Chandra* ACIS-I and S3 observations of NGC 7619 and NGC 7626. The image has been smoothed with an 8″ radius gaussian. For each pointing, regions with less than 10% of the total exposure for that observation were omitted. Point sources have been removed (see text for details). NGC 7619 and NGC 7626 each have a sharp edge in their surface brightness profiles, the former to the northeast, the latter to the southwest. Additionally, NGC 7619 shows a broad tail of stripped gas to the southwest. *Right Panel: DSS* image of the same field.

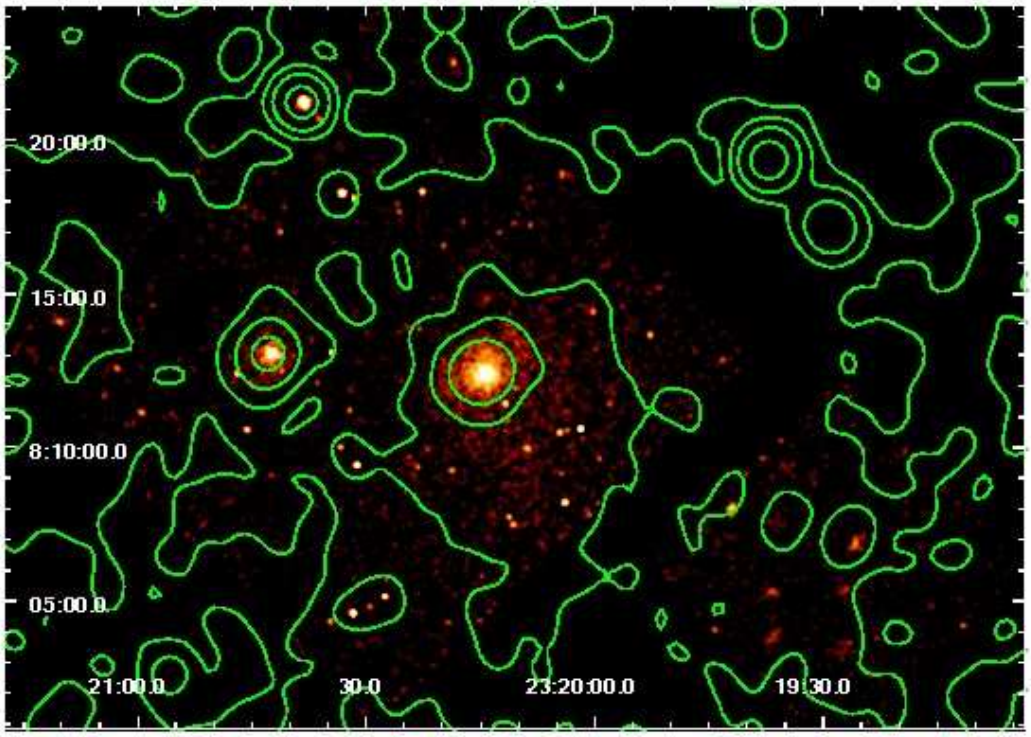

FIG. 2.— *Chandra* 0.6–5 keV mosaic image, including point sources and smoothed with an 8″ radius gaussian, with the logarithmic contours from a soft band *ROSAT* PSPC observation overlain. The ram pressure stripped tail of NGC 7619 is evident, and diffuse emission fills the *Chandra* field of view.

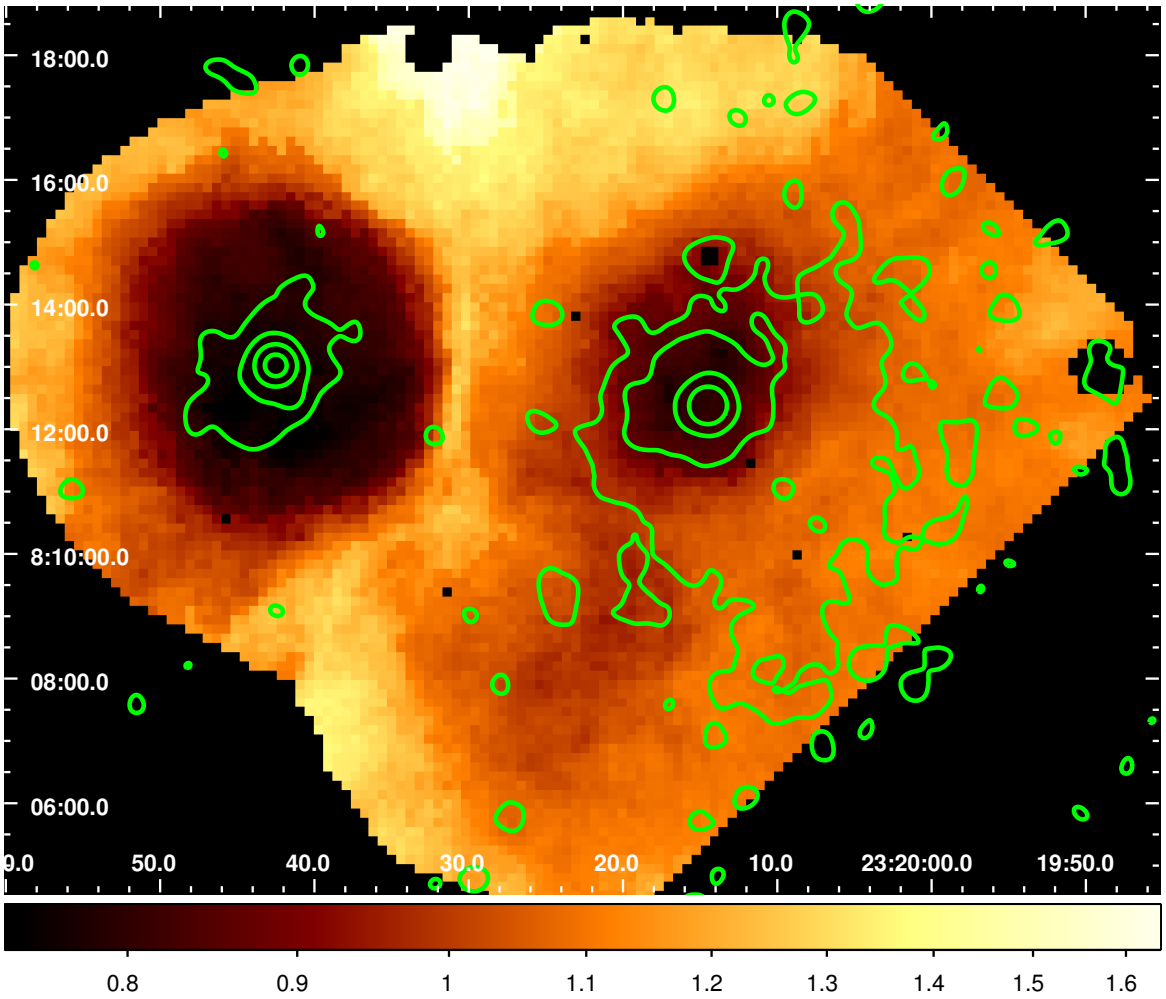

FIG. 3.— Temperature map derived from the ACIS-I observations, with *Chandra* X-ray logarithmic surface brightness contours overlain (with point sources removed). The colorbar gives the temperature in keV. The holes in the temperature map indicate pixels that were completely contained within an excluded source region.

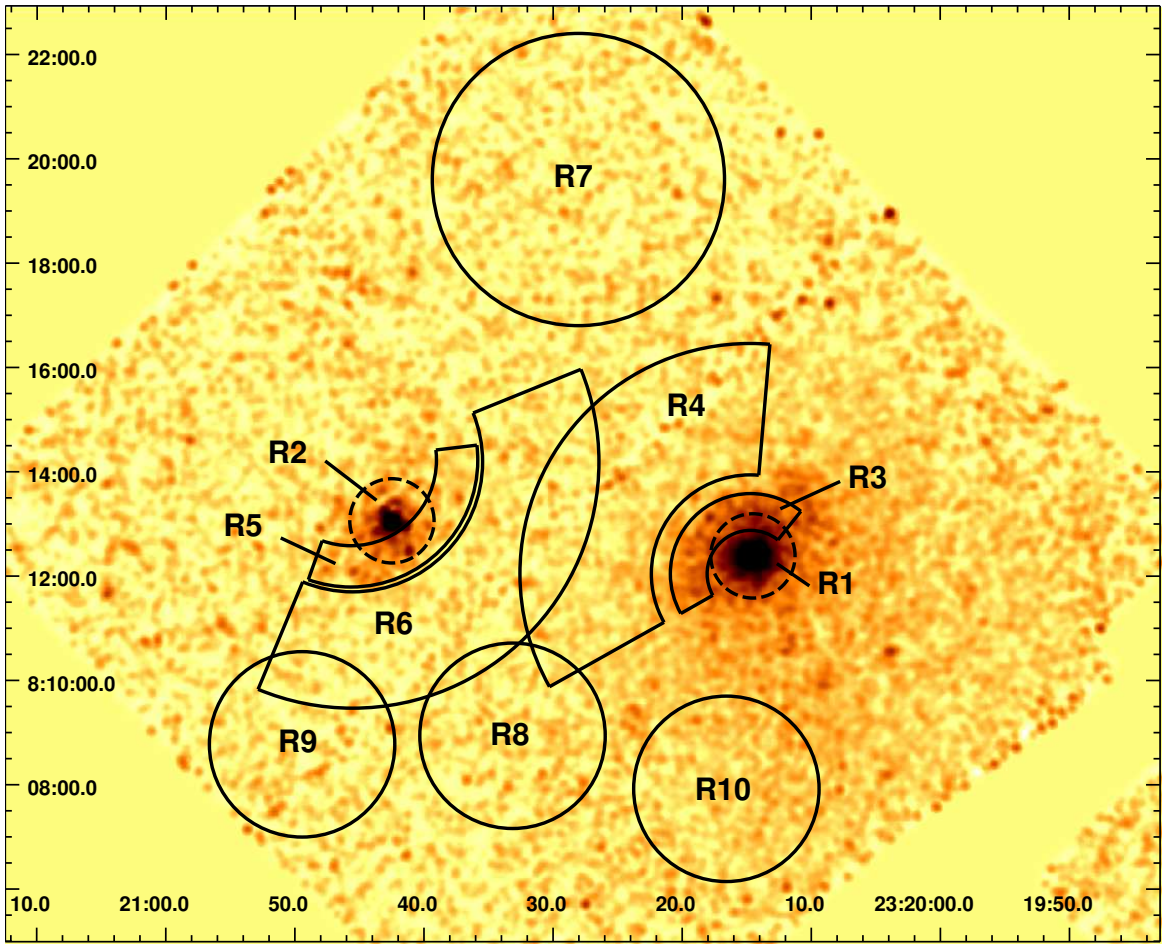

FIG. 4.— The regions fitted in Table 1 overlain on the 0.6 – 5.0 keV merged ACIS-I and S3 *Chandra* image. The image has been smoothed with an 8″ radius gaussian, and the point sources have been removed as described in § 3 of the text.

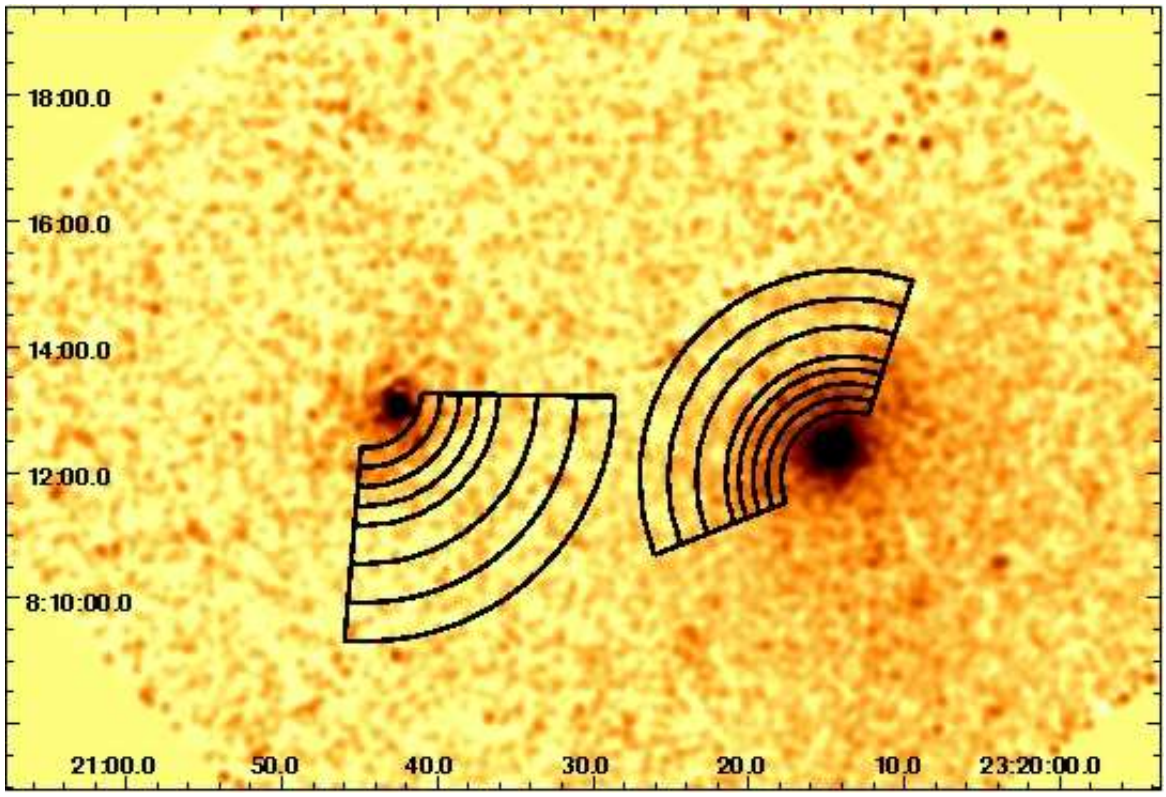

FIG. 5.— A close up view of the central region of Figure 1. The overlain regions indicate the areas used to generate the projected emission measure profiles shown in Figure 6.

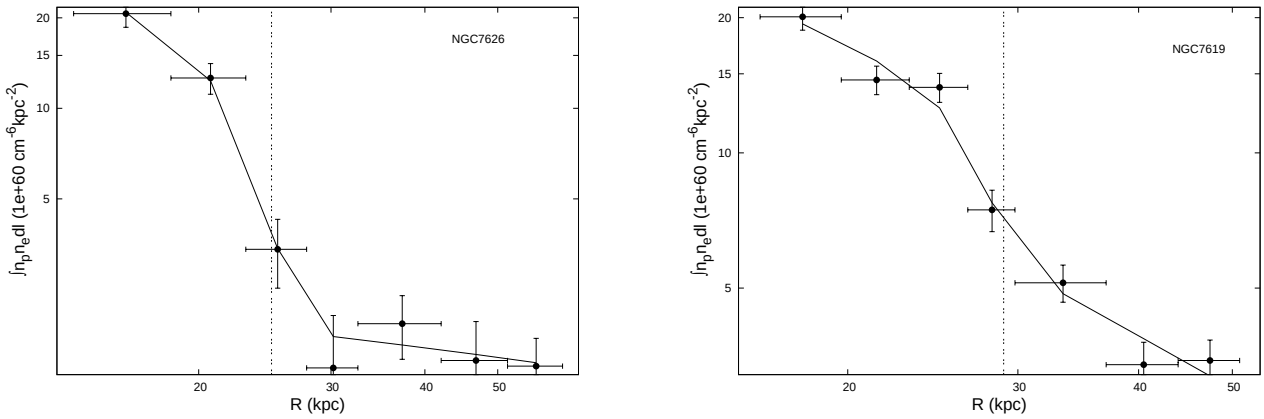

FIG. 6.— *Left Panel:* Integrated emission measure profile across the surface brightness edge in NGC 7626, extracted from the eastern region shown in Figure 5. The x-axis gives the radius from the apparent center of curvature defined by the feature. The best fit two power law density jump model is given by the solid line. The vertical dashed line shows the best fit location of the density discontinuity. *Right Panel:* Same for NGC 7619. Only ACIS-I data were used in each panel.

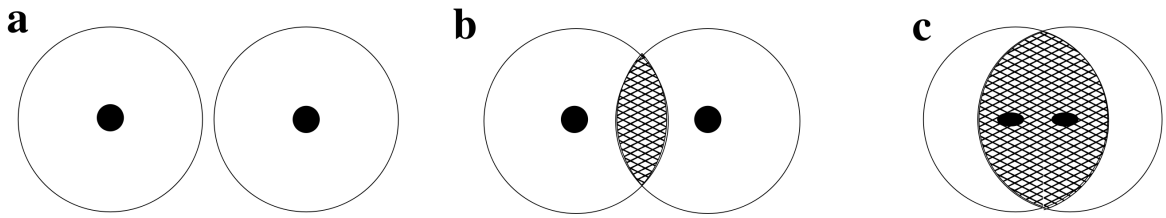

FIG. 7.— Different stages of a merger between two equal mass subgroups. The large circles indicate the virial radii ($\sim$ 0.5 Mpc) of the subgroups, while the filled inner circles indicate the cool gas associated with the central galaxies. *Panel a:* Initially the groups are falling towards one another and the virial radii do not overlap (separation is about 1 Mpc). *Panel b:* The extended halos of the groups merge subsonically and form an intermediate region that is at rest with respect to the center of mass of the system (cross-hatched region). *Panel c:* The relative merger velocity of the subgroups becomes transonic and the galaxies enter the intermediate region, become ram pressure stripped, and form merger cold fronts. The cold fronts indicate the velocities relative to the merged intermediate ICM.

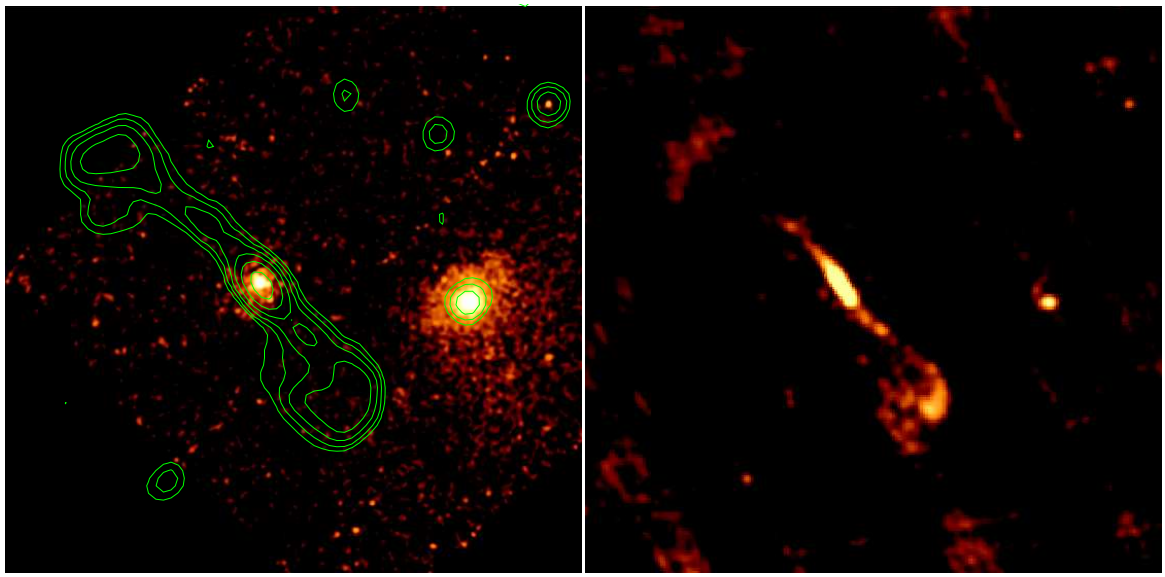

FIG. 8.— *Left Panel:* Close up view of the region near NGC 7626 from Figure 1, with logarithmically spaced NVSS radio contours overlain. The core source, radio jets, and lobes are visible in NGC 7626. The core source in NGC 7619 can be seen in the west. *Right Panel:* Higher-resolution 20 cm VLA observation of the same region. The southern lobe clearly turns back as the jet collides with the ambient ICM.

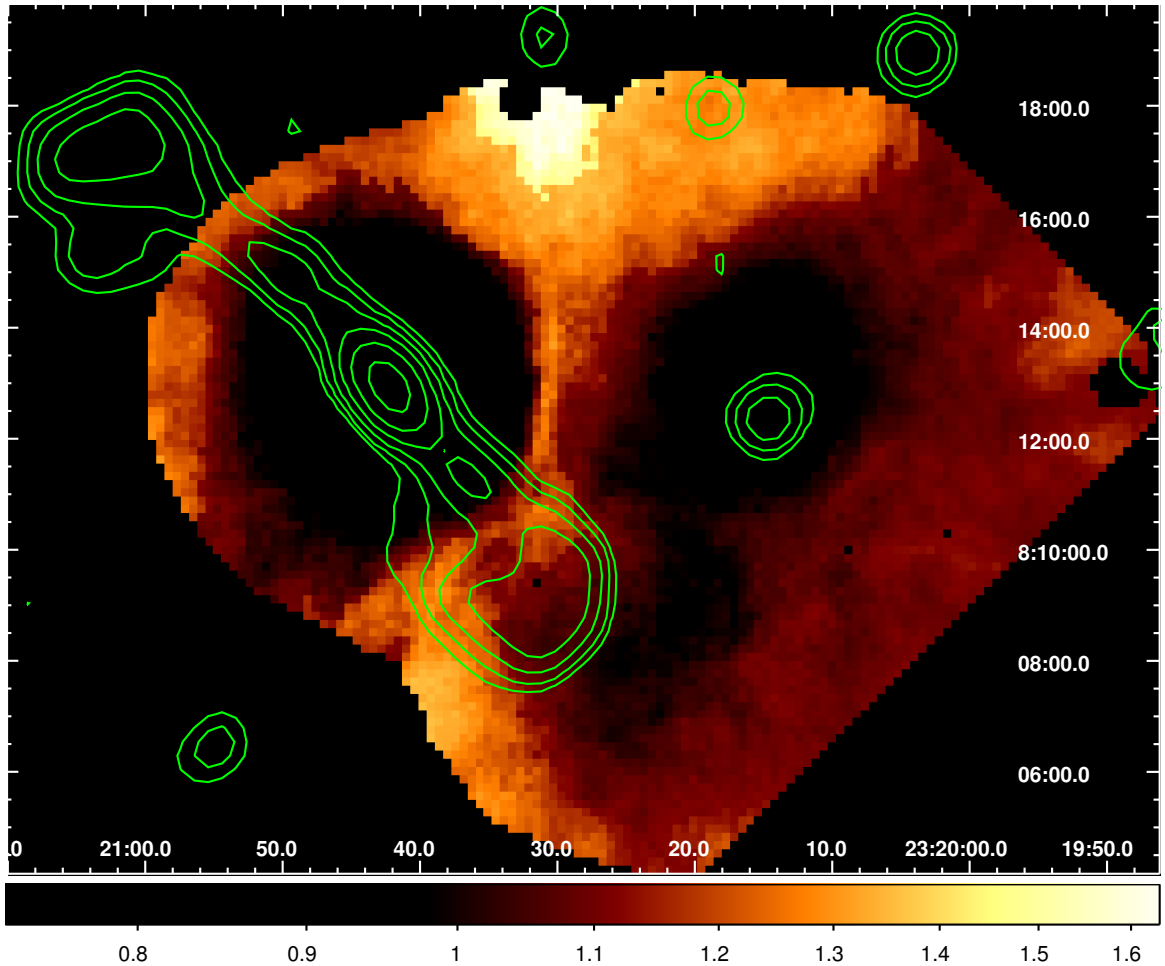

FIG. 9.— Temperature map with the NVSS radio contours overlain. The color bar gives the temperature in keV. A clump of cool gas can be seen just outside the southern radio lobe in NGC 7626, the northern edge of which roughly matches the edge of the lobe. A tongue of intermediate temperature ($\sim$ 1.1 keV) gas extends into the lobe itself.